ROYAL SOCIETY
OF CHEMISTRY

PAPER

Check for updates

Turn-on fluorescent glucose transport bioprobe enables wash-free real-time monitoring of glucose uptake activity in live cells and small organisms†

Monica S. Hensley,[a] David Hutchings,[a] Aldelrahman Ismail[a] and Marina Tanasova ⓘ *[ab]

The direct link between sugar uptake and metabolic diseases highlights the iminent need for molecular tools to detect and evaluate alterations in sugar uptake efficiency as approaches to identify disease-relevant metabolic alterations. However, the strict requirements of facilitative glucose transporters regarding substrate binding and translocation pose challenges for developing effective fluorescence molecular probes. Based on the state-of-the-art understanding of glucose recognition by facilitative transporters (GLUTs), we designed a glucopyranoside mimic – GluRho – that delivers the "turn-on" rhodamine B to live cells *via* glucose transport, including major transporters GLUTs 1–4. The high binding affinity achieved through the secondary interaction between the fluorophore and a GLUT protein supports the delivery of the probe in nutrient-rich conditions, facilitating its use as a tool for a direct assessment of glucose GLUT activity in live cells and organisms and across various experimental settings, including uptake evaluation in the presence of sugars or GLUT activity modulators. The lack of metabolic contribution to the probe uptake due to the elimination of the phosphorylation site contributes to the high efficacy of the GluRho probe in reflecting alterations in glucose uptake efficiency in live cells, between cell lines, and in multicellular model organisms, such as *Drosophila melanogaster*. The molecular modeling analysis of GluRho complexes with GLUT1 and GLUT2 provided essential information on GLUT-probe interactions, highlighting the residues facilitating the effective binding and translocation of the probe through transporters, thus setting the basis for developing glucose-based glycoconjugates as a cargo-delivering platform.

Introduction

Glucose is the primary energy source for most organisms, playing a crucial role in supporting cellular functions through aerobic and anaerobic respiration processes. Glucose, fructose, and other sugars are transported in a gradient-dependent manner into and out of cells through membrane proteins known as facilitative glucose transporters (GLUTs).[1] The role of GLUTs is pivotal in ensuring that cells have a consistent supply of sugars to meet their nutritional needs, supporting processes essential for cell growth and function.

Among the 14 human isoforms of GLUTs, GLUTs 1–4 are the most rigorously characterized glucose transporters. GLUT1 – a

[a] *Department of Chemistry, Michigan Technological University, 1400 Townsend Dr, Houghton, MI 49931, USA. E-mail: mtanasov@mtu.edu*

[b] *Health Research Institute, Michigan Technological University, 1400 Townsend Dr, Houghton, MI 49931, USA*

† Electronic supplementary information (ESI) available: Supporting figures, experimental details, NMR spectra. See DOI: https://doi.org/10.1039/d4cb00239c

ubiquitous glucose transporter, was the first to be characterized, setting a paradigm in the understanding of solute transport.[2] GLUT2 represents the major hepatocyte isoform that also mediates glucose transport in the intestinal tract, liver, kidney, and β-pancreatic cells.[3] GLUT3 is predominantly present in neurons, sperm, and circulating white blood cells.[4,5] GLUT4 is an insulin-dependent transporter present in adipocytes and muscles.[6]

With GLUTs playing a crucial role in the movement of glucose within the body, alterations in GLUT expression and activity have been linked to a broad spectrum of metabolic dysfunctions and diseases, including obesity, diabetes, and cancer.[7] The apparent connection to disease has prompted research into GLUTs as potential targets for developing therapies and diagnostic tools aimed at detecting and treating metabolic diseases. GLUT targeting has been successfully entertained by using sugars and sugar analogs, yielding molecular tools to investigate cellular glucose transport, transporter activity, and glucose metabolism. The ^{3}H, or ^{14}C radiolabeled sugar analogs have been used for decades for the study of

© 2025 The Author(s). Published by the Royal Society of Chemistry

RSC Chem. Biol., 2025, **6**, 987–995 | 987

glucose uptake in the laboratory, providing high sensitivity in glucose uptake measurements,[8–10] and the ^{18}F-labeled glucose has been clinically utilized as trackers for positron emission tomography (PET).[11]

With the development of fluorescence-based detection methods, fluorescence labeling of sugars provided safer, more accessible, and more cost-effective approaches to sugar uptake analysis in laboratory settings. Fluorescent glucose conjugates 6-NBDG and 2-NBDG pioneered the development of fluorescent glucose probes, with conjugates of coumarins, quinolinones, and larger fluorochromes, including near-IR fluorophores,[12–16] further approached for various research contexts, including detecting differences in glucose uptake in live cells and screening sugar uptake inhibitors.[17–19] However, most probes rely on inherently fluorescent chromophores. The characteristic "always on" emission of inherently fluorescent chromophores poses several challenges for real-time activity analysis, requiring the presence of controls for the interpretation of fluorescence results due to background fluorescence and plausible off-target binding. The weak fluorescence intensity is another challenge that can impact the sensitivity of measurements. Compensating for weak fluorescence intensity by increasing probe concentration raises further concerns about impacting normal cellular processes when studying living organisms or cells. In addition, it is essential to note that fluorophore hydrophobicity and H-bonding ability have been found to affect substrate–protein interactions with outcomes ranging from enhanced efficiency of GLUT-mediated uptake to the departure to alternative uptake mechanisms.[14,20,21] For example, the uptake of glucose probes 2-NBDG and 6-NBDG was established to be independent of GLUT1,[20] while the respective C6-coumarin analog of glucose showed a strong dependence on glucose-transporting GLUTs.[22]

In this study, we explored the feasibility of delivering a turn-on fluorophore through glucose-transporting GLUTs to mitigate the limitations in fluorescence imaging of "always-on" fluorophores. To enable real-time fluorescence monitoring, we selected rhodamine B due to its fluorescence emission at long (>600 nm) wavelengths, high quantum yield, and high absorption coefficient. While the spirocyclic form of rhodamine B is non-fluorescent and colorless, protons and metal ions promote the spirolactam opening, stabilizing a strongly fluorescent and pink-colored fluorochrome.[23] Despite the relatively larger size over the NBD or coumarins, the lack of interference with substrate recognition observed upon delivery of rhodamine B through GLUT5[16] provided the feasibility for the effective delivery of a rhodamine fluorophore through glucose-GLUTs, owing to the compliance of the whole conjugate with substrate requirements for GLUT binding and the following translocation. We demonstrate that the conformationally-locked rhodamine-B conjugate of α-D-glucopyranoside (GluRho) is effectively taken up by live cells and small organisms and that the uptake is facilitated by glucose-transporting GLUTs, including major glucose transporters GLUTs 1–4. GluRho uptake exhibits a direct dependence on glucose transport activity, and the turn-on fluorescence enables real-time monitoring of glucose uptake dynamics in cells and small organisms using confocal microscopy and screening of glucose uptake efficiency in cells through flow cytometry.

Results and discussion

### Design, synthesis, and cellular uptake of GluRho

With sugars serving as convenient platforms for GLUT targeting, we based the probe design on glucose while considering the existing information on GLUT-mediated substrate selection for conjugate design.[24] Alterations in glucose structure through substitutions at each of the hydroxyl positions[25,26] supported the formation of hydrogen bonds between the C-1, C-3, and C-4 positions of glucose and polar residues within the transporter protein and hydrophobic interactions with the C-6 position. With glucose equilibrating α- (33%) and β-glucopyranose (66%) anomers in solution, studies of C1-fluoro glucoses explored the capabilities of GLUTs to transport each of the two anomers.[27] The comparative analysis of uptake kinetics for the α and β anomers of the C1 glucopyranosyl fluoride identified the ability of GLUTs to pass both anomers of glucose, with the rate of transport at low substrate concentrations faster for the α anomer. Furthermore, the crystal structure of GLUT3 contains both α and β glucose anomers, with α glucose being more abundant.[28]

In our conjugate design, we envisioned locking the configuration of glucose through methylation at C1–OH. This change would provide the GLUT-preferred pyranoside while maintaining the H-bonding site at C1. For conjugation to the fluorophore, the C6 site of glucoside was targeted, as the presence of C6–OH was found nonessential for the uptake of glucose. Moreover, the lack of C6-hydroxyl eliminates the metabolic contribution to the probe uptake, setting the probe accumulation to report a direct activity of transport. Lastly, with effective uptake identified for α-D-glucopyranoside, we explored rhodamine-B glycoconjugate using α-D-glucopyranoside (GluRho).

The synthesis of GluRho relied on the oxidation of C6–OH of methyl-α-D-glucopyranoside with TEMPO and TCC,[29] followed by the reductive amination of the resulting aldehyde with the primary amine of the rhodamine B hydrazide (Fig. 1A, see ESI,† for synthesis details). The rhodamine B hydrazide (Rho-Hz), in turn, was derived from the rhodamine B through amidation/cyclization with hydrazine hydrate. All intermediates and the final products were characterized and confirmed by ^{1}H and ^{13}C nuclear magnetic resonance spectroscopy (NMR) and high-resolution mass spectrometry (HRMS).

The analysis of GluRho as a glucose uptake probe was carried out in the MCF7 cell line with the established expression of glucose-transporting GLUTs (1, 2, and 4,[30,31] and 12[32]). The Initial evaluations focused on establishing the capability of the probe to turn on fluorescence inside the cell. For this part, MCF7 cells were treated with a range of probe concentrations (1–50 μM) in the complete culture media, and fluorescence was imaged directly after 15 min incubation at 37 °C using confocal microscopy. As a result, GluRho-induced red fluorescence was clearly observable inside the cell at concentrations as low as 1 μM (Fig. 1C). The cell-mediated "turn-on" fluorescence of
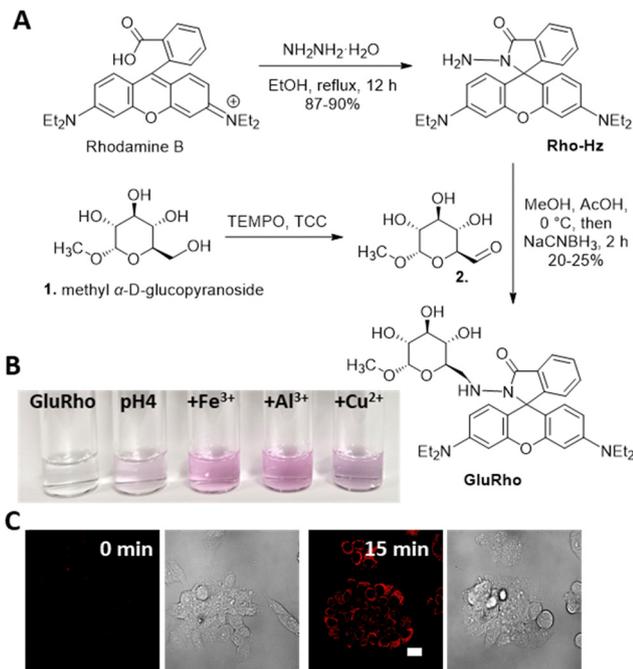
Fig. 1 GluRho synthesis (A), colorimetric change reflecting ion-dependent opening of spirolactam and extension of conjugation (B), and uptake in MCF7 cells (C). For (B), image present GluRho (10 μM in MeOH) in the presence of 1 eq. of the respective ion. For (C), Probe was used at a 2 μM concentration in complete cell culture media. Cells were imaged right after probe addition (time 0 min) at room temperature and after 15 min incubation with the probe at 37 °C. Images were acquired using a confocal microscope, 60× objective, at exc. 559 nm/em. 603 nm under identical imaging parameters. The scale bar is 20 μm.

GluRho was validated by the lack of fluorescence in cells directly after probe addition (Fig. 1C, 0 min) and the culture media in the absence of cells (Fig. S1A, ESI†). GluRho exhibited a concentration-dependent uptake (Fig. S1B, ESI†) that saturated at concentrations >20 μM. Analysis of GluRho uptake at different incubation times (Fig. S2, ESI†) revealed effective accumulation of the probe within 15 min and stability of probe fluorescence for up to 70 min. Specifically, incubating MCF7 cells with GluRho (2 μM, 37 °C) for 10-, 15-, and 30-min resulted in relatively similar fluorescence levels, reflecting the saturation of the uptake within 15 min and the lack of probe efflux. The fluorescence signal remained steady for up to 70 min, reflecting that the equilibration of the probe in the fluorescent open form was complete within the first 15 min of incubation.

We further explored potential initiators of GluRho fluorescence. Rho-Hz derivatives have been documented to turn on in the presence of protons[33] and metal ions, including copper, aluminum, and iron.[34,35] Based on the reported evidence, to identify potential inducers of GluRho fluorescence, the probe was titrated with H^+, Cu^{2+}, Al^{3+}, and Fe^{3+} ions. The colorimetric change to pink (Fig. 1B) reflected an evident capability of GluRho to be activated by different stimuli. Specifically, GluRho fluorescence increased more than twofold in buffered solutions when the pH changed from 7 to 4, indicating its ability to exhibit fluorescence at physiologically relevant pH levels

(Fig. S3, ESI†). When we adjusted the pH of the cell culture media (RPMI) from pH 6 to pH 4 using formic acid, we observed a substantial colorimetric change, corresponding to a >6-fold difference in fluorescence intensity (Fig. S3C, ESI†). It is noteworthy that lowering the pH to 2—whether in a buffered solution or RPMI—resulted in a loss of probe fluorescence and a fading of the pink color (Fig. S3, ESI†). This effect may be due to the protonation of the rhodamine dye, as mass spectrometry analysis revealed no degradation of GluRho (Fig. S4, ESI†).[36]
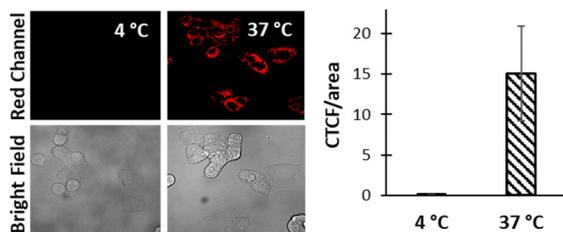
Among the tested metal ions, at an equimolar concentration (10 μM), Fe^{3+} caused >10-fold enhancement of GluRho fluorescence in ACN and MeOH solutions, with fluorescence activation observed at as low as 0.2 equiv. of Fe^{3+}. In an aqueous solution of GluRho, Fe^{3+} produced greater than twofold enhancement of fluorescence (Fig. S5, ESI†). Given the clear activation of GluRho by H^+ at physiological pH and by Fe^{3+} ions at low μM concentrations, it is likely that these two stimuli could contribute to the fluorescence activation of the probe in cells. Additionally, GluRho fluorescence was also turned on by Al^{3+} ions in water and Cu^{2+} ions in MeOH in a concentration-dependent manner (Fig. S5, ESI†).

It is important to note that Rho-Hz was similarly activated by H^+, Fe^{3+}, and Cu^{2+} (Fig. S6, ESI†). Rho-Hz fluorescence demonstrated a significant increase at acidic pH, with more than a sixfold enhancement at pH 4. Rho-Hz fluorescence was turned on in a concentration-dependent manner by 0.2 to 1.8 equiv. of Fe^{3+}. The fluorescence enhancement of Rho-Hz with Cu^{2+} was independent of metal ion concentration, consistent with reports of Rho-Hz hydrolysis to rhodamine B due to Cu^{2+} complexation with the free amine of the hydrazide.[34] Mass spectrometry analysis of the Rho-Hz and Cu^{2+} solution, taken five minutes after the addition of Cu^{2+} (0.4 equiv.), confirmed the hydrolysis of Rho-Hz (Fig. S7, ESI†). In contrast, no signs of hydrolysis were detected in equimolar mixtures of GluRho with Cu^{2+} or Fe^{3+} solutions within 30 minutes after the metal ion addition (Fig. S8, ESI†). The hydrolytic stability of GluRho suggests that the sugar moiety of the glycoconjugate may play a more significant role than the hydrazide in co-chelation with metal ions.

The GluRho conjugate combines a hydrophilic sugar with a hydrophobic fluorophore, prompting us to investigate how the sugar component affects the intracellular accumulation of the probe. To achieve this, we conducted a comparative uptake analysis between the aglycone Rho-Hz and GluRho. MCF7 cells were treated with Rho-Hz for 15 min., and the fluorescence levels were compared to those of GluRho. This analysis was performed using confocal microscopy and flow cytometry (Fig. S9, ESI†). The results showed a strong red fluorescence in the cells treated with GluRho, while there was no detectable accumulation of the aglycone, Rho-Hz, within the 15-min. incubation period. Given the similarities in fluorescence activation between Rho-Hz and GluRho, the absence of fluorescence in the Rho-Hz-treated cells highlights the significant role of the glucose moiety in the translocation of GluRho, implicating GLUT-mediated transport.

To establish the GLUT involvement in GluRho uptake, we explored both the metabolic connection and the specific GLUT

© 2025 The Author(s). Published by the Royal Society of Chemistry

RSC Chem. Biol., 2025, **6**, 987–995 | **989**

Fig. 2 Impact of metabolic activity on GluRho uptake. Fluorescence and bright field images present probe-treated (2 µM) MCF7 cells preconditioned at 37 °C *vs.* 4 °C for 15 min. Images were acquired using a confocal microscope, 60× objective, and recorded at exc. 559 nm/em. 603 nm under identical imaging parameters. Graph presents fluorescence quantified from the respective images using ImageJ as CTCF/Area: CTCF = (Integrated Density − (Area of selected cell × Mean fluorescence of background readings))/Area of the selected cell. Error bars represent the standard deviation.

interactions associated with this process. We determined the metabolic connection in live cells by assessing the temperature dependence of cell metabolism[37] and examining GluRho uptake under conditions that reduced cellular metabolic activity. In this experiment, MCF7 cells were pre-incubated at 4 °C (MCF7$_{cold}$) and subsequently treated with GluRho at 4 °C for 15 min. The uptake of GluRho in MCF7$_{cold}$ culture was completely abolished (Fig. 2), confirming that the uptake of the probe is primarily coupled to the metabolic activity of the cell and indicating a lack of passive diffusion across the cellular membrane.

To determine the specific contributions of glucose transporters (GLUTs), the uptake of GluRho was measured in the presence of competitive substrates and GLUT inhibitors. Cytochalasin B (CytB) is known as a broad GLUT inhibitor with established inhibitory activity towards GLUTs 1–4, 6, 10, and 12.[38,39] Therefore, CytB was used to assess the broader involvement of glucose-transporting GLUTs in GluRho uptake. To assess the specific roles of individual GLUTs, we employed available GLUT-specific competitors (substrates or inhibitors). The contribution from the nonspecific glucose/fructose transporter GLUT2 was assessed using glucosamine (GluAm) as a high-affinity substrate (0.8 mM) and G2iA as a specific inhibitor (IC$_{50}$ ∼ 0.6 µM in the GLUT2-expressing yeast system[40]). Fasentin (IC$_{50(glucose)}$ ∼ 68 µM[41]) was used to delineate GLUT1 and GLUT4 activity. WZB117 (IC$_{50}$ ∼ 0.6 µM[42–44]) and G3iA (K_i ∼ 3.5 µM in GLUT3-expressing yeast system[45]) were used as specific inhibitors of GLUT1 and GLUT3, respectively.

For the inhibition studies, MCF7 cells were incubated with GluRho (0.5 µM) in the presence of the competitor in complete culture medium for 15 min. at 37 °C. To quantify the degree of inhibition, the levels of probe uptake in the absence and presence of competitors were compared (Fig. 3). The results confirmed the involvement of glucose-transporting GLUTs, as indicated by the reduced accumulation of GluRho in the presence of glucose as a competitive substrate. The high glucose concentration (50 mM) required to observe this competition underscored the strong affinity of GluRho for the GLUTs involved in uptake, explaining its effective accumulation in the glucose-rich complete culture medium. The significant
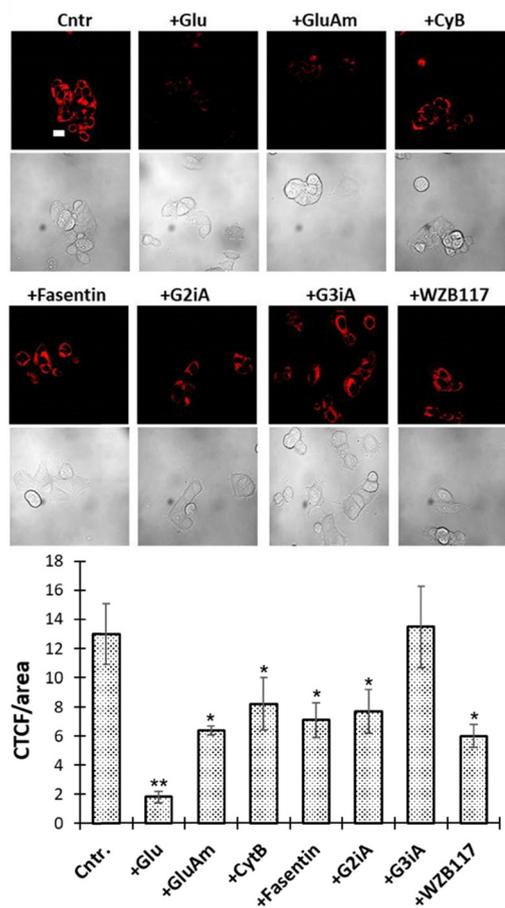
Fig. 3 GluRho (0.5 µM) uptake in MCF7 cells in the presence of inhibitors: glucose (Glu, 50 mM), glucosamine (GluAm) (50 mM), CytB (10 µM), fasentin (100 µM), G2iA (1 µM), G3iA (25 µM), and WZB117 (5 µM). Fluorescence images were acquired using a confocal microscope, 60× objective, and recorded at exc. 559 nm/em. 603 nm under identical imaging parameters. Images were obtained directly after treating MCF7 cells (37 °C, 15 min) with the probe in the absence (cntrl.) or presence of inhibitors. The scale bar is 20 µm. The graph presents fluorescence quantified from the respective images using ImageJ as CTCF/Area: CTCF = (Integrated Density − (Area of selected cell × Mean fluorescence of background readings))/Area of the selected cell. Error bars represent the standard deviation. A two-tailed *t*-test assuming unequal variances was used to detect statistically significant differences as $p < 0.05$: *$p < 0.01$, **$p < 0.001$.

decrease in probe uptake induced by CytB (63% at 10 µM) further highlighted the role of glucose-transporting GLUTs. The specific involvement of GLUT1, GLUT2, and GLUT4 was reflected by the significant reduction in GluRho uptake in the presence of fasentin (55% at 100 µM). Additionally, uptake inhibition by WZB117 (46% at 5 µM) pointed to the involvement of GLUT1, while GluAm (50% at 50 mM) and G2iA (59% at 1 µM) indicated contributions from GLUT2. Conversely, G3iA (10 µM) suggested that GLUT3 had little to no contribution to GluRho uptake, likely due to limited or absent expression of this transporter in MCF7 cells.

To further analyze GluRho as a glucose uptake reporter, we investigated its relationship with GLUT activity enhancement.

990 | *RSC Chem. Biol.*, 2025, **6**, 987–995

© 2025 The Author(s). Published by the Royal Society of Chemistry

Previous studies have shown that an increase in AMPK (AMP-activated protein kinase) activity stimulates GLUT1 and GLUT4 expression, leading to increased GLUT-mediated glucose uptake.[46,47] Therefore, we assessed the relationship between GluRho uptake and AMPK using ampkinone, an AMP kinase activator and glucose uptake enhancer. Following treatment with ampkinone, GluRho uptake increased threefold compared to the untreated control (Fig. S10, ESI†). It is important to note that while glucose uptake in cells is also influenced by changes in the activity of metabolic kinases, the modification of glucoside at the C6–OH position—the phosphorylation site—prevents the consideration of phosphorylation-driven GluRho accumulation. Thus, the observed increase in GluRho uptake indicates the probe's sensitivity to changes in GLUT activity within live cells.

To assess the probe distribution the cells, MCF7 cells were co-treated with solutions containing GluRho and the organelle-specific dyes. Fluorescence imaging was performed using non-overlapping filters (Fig. S11, ESI†). Colocalization studies with the mitochondrial dye MitoView™ revealed accumulation of GluRho in the mitochondria, despite the presence of a sugar moiety, with a Pearson's correlation coefficient of approximately 0.98. Similarly, GluRho exhibited strong accumulation in lysosomes, as assessed through co-incubation with Lysosensor™ Green, yielding a correlation coefficient of around 0.83. Earlier reports highlighted the ability of rhodamine dyes to accumulate in the mitochondria and lysosomes.[48] The observed accumulation of GluRho in both mitochondria and lysosomes suggests the ability of the glycoconjugate to pass through organelle membranes, potentially *via* glucose transport mechanisms.[49] The acidic environment of lysosomes[50] and the high concentration of Fe^{3+} in both lysosomes and mitochondria[51–53] could contribute to the activation of the probe fluorescence in these organelles. The accumulation of GluRho in mitochondria could also be facilitated by its uptake in an open form following spirolactam opening in the cytosol, triggered by H^+, Fe^{3+}, and possibly other stimuli. The mitochondrial accumulation could also be driven by the uptake of GluRho in its open form after spirolactam opening within the cytosol by H^+, Fe^{3+}, and, potentially, other stimuli.[54]

GluRho complexes with GLUTs 1 and 2 follow uptake-relevant H-bonding requirements

To date, the molecular bases of glucose uptake *via* GLUTs are supported by the structural information on human GLUT1, GLUT3,[28,55,56] and bacterial xylose transporter XylE.[57] Molecular docking studies of glucose complexes with a bacterial xylose transporter XylE[57] identified H-bonding of glucose with Gln282 and Gln283 in TM7, Glu384, Pro387, Trp388 in TM10, and Ala407, and Asp411 in TM11. Among those, Glu282, Glu283, and Asp411 were identified to form direct hydrogen bonds with glucose. Successful reproduction of glucose uptake through molecular dynamic simulations[56] using the inward-open crystal structure of human GLUT1,[58] and the homology model of the outward-open GLUT1 generated on the basis of XylE reflected glucose entering the extracellular pocket between TM1, TM2, and TM4, TM7, and TM11 in agreements with the XylE model.
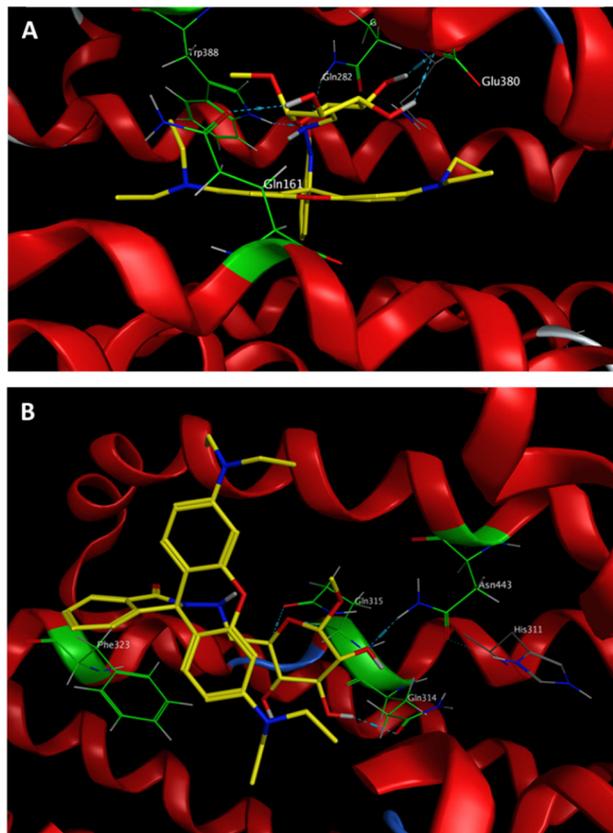
In the entry position, the structure revealed the formation of strong hydrogen bonds with Val69, Arg126, Asn34, and Tyr292. Equilibration in the binding site reflected the rotation of glucose, leading to the formation of hydrogen bonds with Thr30 (TM1), Ser73 (TM2), Tyr292 (TM7), and Asn415 (TM11), and the following stabilization of the hydrogen bonds with Asn288, Asn411, and Gln283. Further direction to the intracellular cavity revealed interactions with Asn411, Asn288, Gln279, Gln282, Gln283, and eventual interaction with Asn415 and Trp412. The structure of human GLUT3 in complex with D-glucose[28] identified polar residues from the C-terminal domain, including Gln280 and Gln281, Asn286, Asn315, Glu378, and Trp386, to coordinate with glucose. The ring oxygen and C1–OH in both anomers are hydrogen-bonded to the side group of Gln159. The α- and β-D-glucose anomers were similarly coordinated by GLUT3 except for the variation at C1–OH. The α- and β-C1–OH are recognized by Trp386 and Gln280, respectively. The carbon backbone of the sugar ring was surrounded by hydrophobic residues, including Phe24, Ile162, Ile166, Ile285, Phe289, and Phe377.

Unlike GLUTs 1 and 3, the understanding of glucose uptake *via* GLUTs 2 and 4 is predominantly provided by experimental studies with glucose analogs. Specifically, similarly to GLUTs 1, 3, and 4, glucose uptake through GLUT2 was found to diminish with alterations at C1, C3, and C4 positions, highlighting their essential role in the recognition and uptake by the transporter. The uptake was not affected by the removal of the C6-hydroxyl.[59]

To obtain structural information about GLUT-GluRho interactions, we proceeded with molecular modeling of GLUT-GluRho complexes. With experimental data implicating GLUTs 1 and 2 in the uptake of GluRho (Fig. 3), we explored the respective models. For GLUT1, the analysis was carried out using the human inward-open GLUT1 ($GLUT1_{in}$, PDB: 4PYP).[58] For GLUT2, we used the homology model generated based on the crystal structure for the human outward-open GLUT3 (PDB: 4ZWC[28]).[40,60] The modeling was carried out using the MOE platform; energy-refined structures for glucose and GluRho were generated, and then the docking poses were generated and refined using a simple scoring function. The GLUT structure was kept rigid during the docking step.

The GLUT1 complexes with glucose reflected the binding interactions identified in prior studies. Namely, glucose binding within the $GLUT1_{in}$ was found to involve Gln283, Asn288, Gln380, Trp388, Asn411, Trp412, and Asn415 (Fig. S12, ESI†). Analysis of poses accommodated by glucose within the binding site highlighted a predominant contribution of Gln283, Asn288, and Trp388 to glucose-GLUT1 complexation. Docking analysis of GluRho also revealed that the probe binds within the designated site, despite its larger size (Fig. 4). However, compared to the glucose-GLUT1 complex, GluRho orients the spirocyclic amide of the rhodamine moiety towards the preferred glucose-binding site (Fig. S12, ESI†). This orientation is stabilized by strong hydrogen bonding with Gln282 (not present for glucose) and is further enhanced by interactions with Trp388. In addition, the hydrogen bonding network supported by Gln161 and Gln380 involves the glucose moiety. A summary of the interactions for

© 2025 The Author(s). Published by the Royal Society of Chemistry

RSC Chem. Biol., 2025, **6**, 987–995 | **991**

Fig. 4 Docking of GluRho within GLUT1$_{in}$ (A) and GLUT2$_{out}$ (B). For (A), the human inward-open GLUT1 (PDB: 4PYP) structure was used. For (B), an outward-open GLUT2 homology model was constructed based on the human outward-open GLUT3 structure (PDB: 4ZWC). Docking performed using MOE. Images generated using MOE.

each pose of GluRho within GLUT1 indicates that Gln282, Gln380, and Trp388 are key amino acids contributing to the formation of the complex *via* relevant hydrogen bonding interactions.

For GLUT2, we identified that the glucose-GLUT2 complex is stabilized by the contributions of Gln193, Gln315, Gln412, Trp420, and Asn443 (Fig. S13, ESI†). When we docked GluRho within the GLUT2$_{out}$, the probe was positioned in the glucose binding site, allowing the sugar moiety to interact in a manner similar to glucose (Fig. S13, ESI†). In addition to significant hydrogen bonding with Gln315 and Asn443, the rhodamine portion of the probe was oriented toward the hydrophobic pocket within the substrate binding site. This complex was further stabilized by aromatic interactions with Phe323, supporting the higher affinity of GluRho over glucose.

Overall, the orientation and binding of GluRho, similar to that of glucose, within the outward-open conformation indicate that the probe can feasibly translocate through the transporter during the relevant conformational change from GLUT$_{out}$ to GLUT$_{in}$. Conversely, the differing orientation and binding of GluRho from glucose in the inward-open conformation suggest that the conformational change from GLUT$_{in}$ to GLUT$_{out}$ is less likely to occur. This discrepancy helps explain the probe's stable uptake levels and its lack of efflux.

## GluRho as a glucose uptake reflector in live cells and organisms

In this study, we investigated the feasibility of detecting differences in GluRho uptake among cells with varying GLUT expression profiles. The uptake was carried out using flow cytometry to facilitate the throughput of analysis. Initially, we compared the uptake of GluRho in MCF7 cells using both confocal microscopy and flow cytometry. After imaging GluRho accumulation in MCF7 cells with a confocal microscope, probe-treated cells were collected and analyzed with the flow cytometer. The concentration-dependent analysis (ranging from 1 to 50 μM) indicated that probe uptake reached saturation after 25 μM in both imaging methods (Fig. S14A and B, ESI†). Subsequently, we evaluated the probe uptake in HeLa cells (cervical cancer) and MDA-MB-231 cells (triple-negative breast cancer). The uptake of GluRho increased in both cell lines within the 1 to 25 μM concentration range (Fig. 5), with saturation also observed after 25 μM (Fig. S14, ESI†).

The comparative analysis of probe uptake efficiency within a concentration range 1–25 μM revealed an evident impact of probe concentration on uptake. Since GluRho exhibits non-specific uptake mediated by glucose transporters (GLUTs), the observed differences in concentration-dependent uptake among cells can be attributed to the involvement of GLUTs with varying affinities and transport capacities. For instance, MCF7 cells express GLUTs, 1, 2, and 4,[30,31] and 12,[32] while HeLa and MDA-MB-231 cells were identified to express GLUTs 1 and 3.[49,61] The uptake kinetics analysis in oocytes suggested GLUT3 to be of higher affinity to D-glucose than GLUT1 ($K_{m(glucose)} \sim 3$ mM).[62] Recent *in vitro* D-glucose kinetics studies in a reconstituted-liposome system demonstrated that GLUT1 and GLUT3 have relatively similar K_m values (1.4 mM for GLUT3 and 2.0 mM for GLUT1), but GLUT3 exhibits a higher turnover.[63] GLUT4 has a reported $K_{m(glucose)} \sim 5$ mM,[63,64] which is higher than that of GLUT1, and it has a very slow turnover,[63] likely to facilitate insulin-dependent uptake regulation. GLUT2, on the other hand, has a low affinity ($K_{m(glucose)} \sim 17$ mM) but a high capacity for D-glucose uptake.[65] Consequently, at low GluRho concentrations, we would expect the predominant involvement of higher-affinity transporters such as GLUT1 and
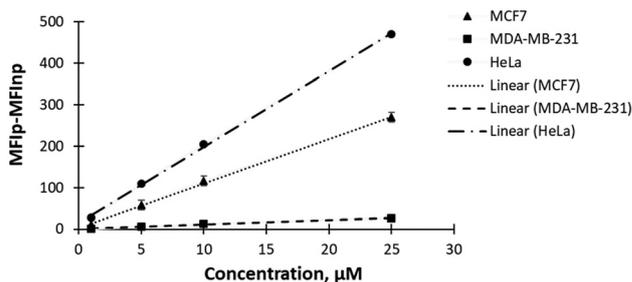
Fig. 5 Analysis of GluRho (1–25 μM) uptake in MCF7, MDA-MB-231, and HeLa cells. The uptake was evaluated using Attune NxT flow cytometer after 10 min cell treatment with GluRho at 37 °C. Fluorescence was quantified as the difference in MFI between cells treated with the probe (MFIp) − untreated cells (MFInp). Measurements were carried out using a YL2 filter for 1000 cells per concentration. Data represents the average fluorescence for three repeats. Fluorescence is presented as dark markers. Lines represent the linear fit (Excel).
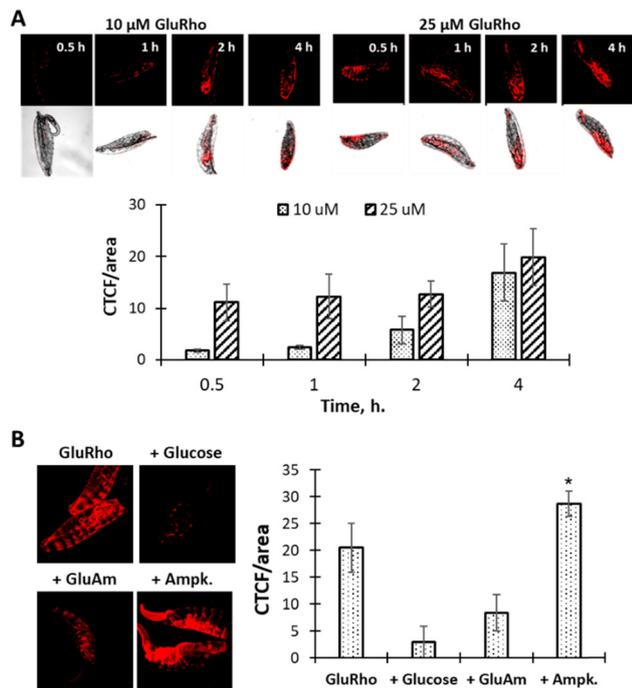
Fig. 6 GluRho uptake in *Drosophila melanogaster* larvae. (A) Probe uptake over time and concentrations. (B) Probe uptake in the presence of competitor glucose (Glucose) and glucosamine (GluAm), and glucose uptake inducer ampkinone (Ampk.). Larvae were imaged using a confocal microscope, 10× objective. Fluorescence recorded at exc. 559 nm/em. 603 nm. Graphs represent probe-induced fluorescence quantified from the respective confocal images using ImageJ as CTCF/Area: CTCF = (Integrated Density − (Area of selected cell × Mean fluorescence of background readings))/Area of the selected cell. Error bars represent the standard deviation. A two-tailed *t*-test assuming unequal variances was used to detect statistically significant differences as $p < 0.05$: $p^* < 0.001$.

GLUT3 in the probe uptake. Once the uptake by GLUT1 and GLUT3 reaches saturation, an increase in probe concentration would likely lead to the involvement of lower-affinity glucose transporters, such as GLUT4 and then GLUT2, along with the potential participation of other glucose transporters.

To determine whether GluRho can detect changes in glucose uptake in multicellular organisms, we investigated its uptake in *Drosophila melanogaster* larvae. *Drosophila melanogaster* has been established to express Glut1 (ubiquitous expression) and Glut3 (expressed in testes),[66] and has been successfully used as a model for metabolic diseases.[67] In our study, larvae were treated with a PBS-based GluRho solution over different time intervals and concentrations. The probe-treated larvae were mounted on a glass slide and imaged with a confocal microscope. As shown in Fig. 6, probe-induced fluorescence was observable at about 0.5 h with 10 μM concentration of GluRho, and the fluorescence intensity increased with an extension of incubation time from 0.5 h to 4 h. When the probe concentration was raised to 25 μM, we observed substantially higher levels of probe accumulation within the cells. However, at higher concentrations of GluRho, the time-dependence of the uptake between 0.5 and 2 h. diminished, likely due to the simultaneous involvement of multiple GLUT transporters

leading to uptake saturation. For both concentrations tested, the uptake reached similar levels after 4 hours.

The dependence of probe uptake on sugar transporters in the larvae was confirmed by reduction in fluorescence accumulation when competitors were present (Fig. 6B). Specifically, fluorescence accumulation decreased by over 80% when 50 mM glucose was introduced, while glucosamine (GluAm) led to a greater than 50% reduction in GluRho uptake. Additionally, ampkinone was found to significantly enhance the uptake of the probe, underscoring the relationship between GLUT activity and GluRho uptake.

Conclusions

In this study, we developed a turn-on bioprobe – GluRho – for monitoring *in vitro* and *in vivo* GLUT-mediated transport. Despite the large size of the fluorophore, the glucose conjugate of rhodamine B hydrazide is effectively accumulated in live cells *via* facilitative glucose transporters (GLUTs). Probe accumulation was reflected by the appearance of red fluorescence visible only inside the cell, reflecting the cell-mediated opening of the rhodamine B spirolactam and the in-cell formation of the conjugated fluorescence system. Importantly, the lack of probe fluorescence in the culture media allows for analyses to be conducted without the need for post-incubation washes, making GluRho suitable for high-throughput screening of glucose transport activity. The probe effectively competes for uptake with glucose, and its accumulation is achievable even in complete cell culture media. We observed the turn-on fluorescence develop rapidly, with the fluorescence signal equilibrating within 15 min. The effective response of the turn-on signal also enabled comparative analysis of GLUT activity in MCF7 cells in the presence of GLUT inhibitors, confirming the roles of GLUTs 1 and 2 in the accumulation of the probe. Molecular modeling analysis of glucose and GluRho complexes with GLUTs 1 and 2 showed that the probe-GLUT interaction is stabilized by uptake-relevant residues, supporting the GLUT-mediated passage of GluRho. The ability of GluRho to reflect changes in glucose uptake efficiency in live cells was validated by observing enhanced uptake in response to AMPK-mediated changes in glucose transport activity. As a glucose uptake reporter, GluRho effectively shows differences in glucose uptake efficiency between various cell lines. Additionally, the stability of the probe's fluorescence for at least two hours supports its use in assessing glucose uptake in smaller organisms, such as *Drosophila melanogaster* larvae. Notable changes in GluRho uptake levels in response to glucose, glucosamine, and ampkinone further confirm GluRho as an effective reporter of glucose uptake activity *in vivo*.

Author contributions

M. S. H. designed and synthesized the probe, M. S. H. and D. H. performed experiments, I. S. performed modelling studies, M. T. led the studies, M. S. H. and M. T. wrote the manuscript. All authors reviewed the manuscript.

© 2025 The Author(s). Published by the Royal Society of Chemistry

RSC Chem. Biol., 2025, **6**, 987–995 | **993**

Data availability

Additional Data Figures, Experimental details, and NMR characterization is provided as Supported Information. Data is also available on demand.

Conflicts of interest

There are no conflicts to declare.

Acknowledgements

References

1 W. Long and C. I. Cheeseman, *Dovepress*, 2015, **7**, 167–183.
2 B. Thorens and M. Mueckler, *Am. J. Physiol.: Endocrinol. Metab.*, 2010, **298**, E141–E145.
3 B. Thorens, H. K. Sarkar, H. R. Kaback and H. F. Lodish, *Cell*, 1988, **55**, 281–290.
4 B. Wang, S. Lorente-Cebrian, E. Rodriguez, S. Wood and P. Trayhurn, *Int. J. Obes.*, 2007, **31**, S49–S49.
5 I. A. Simpson, D. Dwyer, D. Malide, K. H. Moley, A. Travis and S. J. Vannucci, *Am. J. Physiol.: Endocrinol. Metab.*, 2008, **295**, E242–E253.
6 D. E. James, R. Brown, J. Navarro and P. F. Pilch, *Nature*, 1988, **333**, 183–185.
7 K. M. Gillespie, E. Kemps, M. J. White and S. E. Bartlett, *Nutrients*, 2023, **15**, 889.
8 N. Baker, *Diabetes*, 1956, **5**, 178–186.
9 A. Virkamaki, E. Rissanen, S. Hamalainen, T. Utriainen and H. YkiJarvinen, *Diabetes*, 1997, **46**, 1106–1110.
10 A. C. Ho-Palma, F. Rotondo, M. D. Romero, J. A. Fernández-López, X. Remesar and M. Alemany, *Adipocyte*, 2018, **7**, 204–217.
11 M. M. Graham, R. L. Wahl, J. M. Hoffman, J. T. Yap, J. J. Sunderland, R. Boellaard, E. S. Perlman, P. E. Kinahan, P. E. Christian, O. S. Hoekstra and G. S. Dorfman, *J. Nucl. Med.*, 2015, **56**, 955–961.
12 Z. Cheng, J. Levi, Z. Xiong, O. Gheysens, S. Keren, X. Chen and S. S. Gambhir, *Bioconjugate Chem.*, 2006, **17**, 662–669.
13 S. G. Chen, Y. F. Fang, Q. W. Zhu, W. L. Zhang, X. W. Zhang and W. Lu, *RSC Adv.*, 2016, **6**, 81894–81901.
14 V. V. Begoyan, L. J. Weselinski, S. Xia, J. Fedie, S. Kannan, A. Ferrier, S. Rao and M. Tanasova, *Chem. Commun.*, 2018, **54**, 3855–3858.
15 S. Benson, A. Fernandez, N. D. Barth, F. de Moliner, M. H. Horrocks, C. S. Herrington, J. L. Abad, A. Delgado, L. Kelly, Z. Chang, Y. Feng, M. Nishiura, Y. Hori, K. Kikuchi and M. Vendrell, *Angew. Chem., Int. Ed.*, 2019, **58**, 6911–6915.
16 M. M. S. Nyansa, A. Oronova, N. Gora, M. R. Geborkoff, N. R. Ostlund, D. R. Fritz, T. Werner and M. Tanasova, *Chem. Biomed. Imaging*, 2023, **1**, 637–647.
17 S. Kannan, V. V. Begoyan, J. R. Fedie, S. Xia, L. J. Weselinski, M. Tanasova and S. Rao, *Biosensors*, 2018, **8**, e39–e50.
18 A. Oronova and M. Tanasova, *Int. J. Mol. Sci.*, 2023, **24**, 173–187.
19 T. Y. Kao, H. W. Wu, S. S. Lee, P. H. Liang, J. H. Guh and L. C. Hsu, *J. Food Drug Anal.*, 2021, **29**, 521–532.
20 K. E. Hamilton, M. F. Bouwer, L. L. Louters and B. D. Looyenga, *Biochimie*, 2021, **190**, 1–11.
21 N. Nahrjou, A. Ghosh and M. Tanasova, *Int. J. Mol. Sci.*, 2021, **22**, 5073.
22 Y. Otsuka, A. Sasaki, T. Teshima, K. Yamada and T. Yamamoto, *Org. Lett.*, 2016, **18**, 1338–1341.
23 H. N. Kim, M. H. Lee, H. J. Kim, J. S. Kim and J. Yoon, *Chem. Soc. Rev.*, 2008, **37**, 1465–1472.
24 G. D. Holman, *Pflugers Arch.*, 2020, **472**, 1155–1175.
25 J. E. Barnett, G. D. Holman and K. A. Munday, *Biochem. J.*, 1973, **135**, 539–541.
26 A. Kahlenberg and D. Dolansky, *Can. J. Biochem.*, 1972, **50**, 638–643.
27 R. E. London and S. A. Gabel, *Biophys. J.*, 1995, **69**, 1814–1818.
28 D. Deng, P. C. Sun, C. Y. Yan, M. Ke, X. Jiang, L. Xiong, W. L. Ren, K. Hirata, M. Yamamoto, S. L. Fan and N. Yan, *Nature*, 2015, **526**, 391–396.
29 M. Angelin, M. Hermansson, H. Dong and O. Ramström, *Eur. J. Org. Chem.*, 2006, 4323–4326.
30 J. Levi, Z. Cheng, O. Gheysens, M. Patel, C. T. Chan, Y. B. Wang, M. Namavari and S. S. Gambhir, *Bioconjugate Chem.*, 2007, **18**, 628–634.
31 A. M. Barbosa and F. Martel, *Cancers*, 2020, **12**, 154.
32 M. L. Macheda, S. Rogers and J. D. Best, *J. Cell. Physiol.*, 2005, **202**, 654–662.
33 S. Kang, S. Kim, Y. K. Yang, S. Bae and J. Tae, *Tetrahedron Lett.*, 2009, **50**, 2010–2012.
34 V. Dujols, F. Ford and A. W. Czarnik, *J. Am. Chem. Soc.*, 1997, **119**, 7386–7387.
35 W. Q. Xu, F. Ahmed and H. Xiong, *Anal. Chim. Acta*, 2023, **1249**, 340925.
36 I. Moreno-Villoslada, M. Jofré, V. Miranda, R. González, T. Sotelo, S. Hess and B. L. Rivas, *J. Phys. Chem. B*, 2006, **110**, 11809–11812.
37 F. A. Smith, *J. Exp. Bot.*, 1967, **18**, 348–358.
38 R. Augustin, *IUBMB Life*, 2010, **62**, 315–333.
39 K. Kapoor, J. S. Finer-Moore, B. P. Pedersen, L. Caboni, A. Waight, R. C. Hillig, P. Bringmann, I. Heisler, T. Müller, H. Siebeneicher and R. M. Stroud, *Proc. Natl. Acad. Sci. U. S. A.*, 2016, **113**, 4711–4716.
40 S. Schmidl, O. Ursu, C. V. Iancu, M. Oreb, T. I. Oprea and J. Y. Choe, *Sci. Rep.*, 2021, **11**, 13751.
41 T. E. Wood, S. Dalili, C. D. Simpson, R. Hurren, X. L. Mao, F. S. Saiz, M. Gronda, Y. Eberhard, M. D. Minden, P. J. Bilan, A. Klip, R. A. Batey and A. D. Schimmer, *Mol. Cancer Ther.*, 2008, **7**, 3546–3555.
42 Y. Liu, Y. Cao, W. Zhang, S. Bergmeier, Y. Qian, H. Akbar, R. Colvin, J. Ding, L. Tong, S. Wu, J. Hines and X. Chen, *Mol. Cancer Ther.*, 2012, **11**, 1672–1682.

43 O. A. Ojelabi, K. P. Lloyd, A. H. Simon, J. K. De Zutter and A. Carruthers, *J. Biol. Chem.*, 2016, **291**, 26762–26772.

44 W. H. Zhang, Y. Liu, X. Z. Chen and S. C. Bergmeier, *Bioorg. Med. Chem. Lett.*, 2010, **20**, 2191–2194.

45 C. V. Iancu, G. Bocci, M. Ishtikhar, M. Khamrai, M. Oreb, T. I. Oprea and J. Y. Choe, *Sci. Rep.*, 2022, **12**, 1429.

46 E. J. Kurth-Kraczek, M. F. Hirshman, L. J. Goodyear and W. W. Winder, *Diabetes*, 1999, **48**, 1667–1671.

47 L. G. Fryer, F. Foufelle, K. Barnes, S. A. Baldwin, A. Woods and D. Carling, *Biochem. J.*, 2002, **363**, 167–174.

48 X. Chen, T. Pradhan, F. Wang, J. S. Kim and J. Yoon, *Chem. Rev.*, 2012, **112**, 1910–1956.

49 S. J. Qualls-Histed, C. P. Nielsen and J. A. MacGurn, *iScience*, 2023, **26**, 106150.

50 S. Ohkuma and B. Poole, *Proc. Natl. Acad. Sci. U. S. A.*, 1978, **75**, 3327–3331.

51 B. T. Paul, D. H. Manz, F. M. Torti and S. V. Torti, *Expert. Rev. Hematol.*, 2017, **10**, 65–79.

52 F. Rizzollo, S. More, P. Vangheluwe and P. Agostinis, *Trends Biochem. Sci.*, 2021, **46**, 960–975.

53 D. R. Richardson, D. J. R. Lane, E. M. Becker, M. L. H. Huang, M. Whitnall, Y. S. Rahmanto, A. D. Sheftel and P. Ponka, *Proc. Natl. Acad. Sci. U. S. A.*, 2010, **107**, 10775–10782.

54 C. C. Philpott and S. Jadhav, *Free Radical Bio. Med.*, 2019, **133**, 112–117.

55 P. W. Hruz and M. M. Mueckler, *Mol. Membr. Biol.*, 2001, **18**, 183–193.

56 T. Galochkina, M. N. F. Chong, L. Challali, S. Abbar and C. Etchebest, *Sci. Rep.*, 2019, **9**, 998.

57 X. Fu, G. Zhang, R. Liu, J. Wei, D. Zhang-Negrerie, X. Jian and Q. Gao, *J. Chem. Inf. Model.*, 2016, **56**, 517–526.

58 D. Deng, C. Xu, P. C. Sun, J. P. Wu, C. Y. Yan, M. X. Hu and N. Yan, *Nature*, 2014, **510**, 121–125.

59 C. A. Colville, M. J. Seatter, T. J. Jess, G. W. Gould and H. M. Thomas, *Biochem. J.*, 1993, **290**(Pt 3), 701–706.

60 N. Gora, L. J. Weselinski, V. V. Begoyan, A. Cooper, J. Y. Choe and M. Tanasova, *ACS Chem. Biol.*, 2023, **18**, 1089–1100.

61 R. A. Medina and G. I. Owen, *Biol. Res.*, 2002, **35**, 9–26.

62 G. W. Gould, H. M. Thomas, T. J. Jess and G. I. Bell, *Biochemistry*, 1991, **30**, 5139–5145.

63 A. Suades, A. Qureshi, S. E. McComas, M. Coincon, A. Rudling, Y. Chatzikyriakidou, M. Landreh, J. Carlsson and D. Drew, *Nat. Commun.*, 2023, **14**, 4070.

64 T. Wang, J. Wang, X. Hu, X. J. Huang and G. X. Chen, *World J. Biol. Chem.*, 2020, **11**, 76–98.

65 S. Schmidl, S. T. A. Rojas, C. V. Iancu, J. Y. Choe and M. Oreb, *Front. Mol. Biosci.*, 2021, **7**, 598419.

66 V. R. Chintapalli, J. Wang and J. A. Dow, *Nat. Genet.*, 2007, **39**, 715–720.

67 P. Graham and L. Pick, *Curr. Top. Dev. Biol.*, 2017, **121**, 397–419.

© 2025 The Author(s). Published by the Royal Society of Chemistry

RSC Chem. Biol., 2025, **6**, 987–995 | **995**